Title

Soil carbon dioxide emissions due to oxidative peat decomposition in an oil palm plantation on tropical peat

Journal name

Agriculture, Ecosystems & Environment

Type of paper

Original paper

Author names and affiliations

Kiwamu Ishikura[1], Takashi Hirano[1], Yosuke Okimoto[1], Ryuichi Hirata[2], Frankie Kiew[1,3], Lulie Melling[3], Edward Baran Aeries[3], Kim San Lo[3], Kevin Kemudang Musin[3], Joseph Wenceslaus Waili[3], Guan Xhuan Wong[1,3], Yoshiyuki Ishii[4]

[1]Research Faculty of Agriculture, Hokkaido University, Kita-ku, Kita 9, Nishi 9, Sapporo, Hokkaido 060-8589, Japan

[2]Center for Global Environmental Research, National Institute for Environmental Studies, Tsukuba, Ibaraki 305-8506, Japan

[3]Sarawak Tropical Peat Research Institute, Lot 6035, Kuching – Kota Samarahan Expressway, 94300 Kota Samarahan, Sarawak, Malaysia

[4]Institute of Low Temperature Science, Hokkaido University, Kita-ku, Kita 19, Nishi 8, Sapporo, Hokkaido 060-0819, Japan

Corresponding author: Kiwamu Ishikura

Current postal address: Laboratory of Ecological and Environmental Physics, Research Faculty of Agriculture, Hokkaido University, Kita-ku, Kita 9, Nishi 9, Sapporo, Hokkaido 060-8589, Japan

E-mail address: ishikura@chem.agr.hokudai.ac.jp

Abstract

Soil carbon dioxide (CO_2) efflux was measured continuously for two years using an automated chamber system in an oil palm plantation on tropical peat. This study investigated the factors controlling the CO_2 efflux and quantified the annual cumulative CO_2 emissions through soil respiration and heterotrophic respiration, which is equivalent to oxidative peat decomposition. Soil respiration was measured in close-to-tree (<2.5 m, CT) and far-from-tree (>3 m, FT) plots, and heterotrophic respiration was measured in root-cut (RC) plots by a trenching method. The daily mean CO_2 efflux values (mean ± 1 standard deviation) were 2.80 ± 2.18, 1.59 ± 1.18, and 1.94 ± 1.58 μmol m^{-2} s^{-1} in the CT, FT, and RC plots, respectively. Daily mean CO_2 efflux increased exponentially as the groundwater level or water-filled pore space decreased, indicating that oxidative peat decomposition and gas diffusion in the soil increased due to enhanced aeration resulting from lower groundwater levels. Mean annual gap-filled CO_2 emissions were 1.03 ± 0.53, 0.59 ± 0.26, and 0.69 ± 0.21 kg C m^{-2} yr^{-1} in the CT, FT, and RC plots, respectively. Soil CO_2 emissions were significantly higher in the CT plots ($P < 0.05$), but did not differ significantly between the FT and RC plots. This implies that root respiration was negligible in the FT plots. Heterotrophic respiration accounted for 66% of soil respiration. Annual CO_2 emissions through both soil and heterotrophic respiration were smaller than those of other oil palm plantations on tropical peat, possibly due to the higher groundwater levels, land compaction, and continuous measurement of soil CO_2 efflux in this study. Mean annual total subsidence was 1.55 to 1.62 cm yr^{-1}, of which oxidative peat decomposition accounted for 72 to 74%. In conclusion, water management to raise groundwater levels would mitigate soil CO_2 emissions from oil palm plantations on tropical peatland.

Keywords

Automated chamber system; Carbon dioxide efflux; Groundwater level; Heterotrophic respiration; Soil respiration; Subsidence; Trenching

1. Introduction

Peatland stocks approximately one-third of the global terrestrial carbon (C) in 3% of the global terrestrial area (Maltby and Immirzi, 1993), and approximately 25 Mha are in Southeast Asia, especially in Indonesia and Malaysia (Page et al., 2011). However, tropical peatland has been rapidly reclaimed since the 1990s, mainly for oil palm and *Acacia* plantations. By 2015, oil palm plantations had expanded to cover an area of 4.3 Mha on peat in Indonesia and Malaysia (Miettinen et al., 2016). Because the agricultural use of tropical peatland is commonly accompanied by drainage, the aerobic mineralization of peat soil is promoted, resulting in large carbon dioxide (CO_2) emissions (e.g., Furukawa et al., 2005; Couwenberg et al., 2010; Hooijer et al., 2012). Peat is usually compacted using heavy machinery before planting in Malaysia to enhance its bearing capacity for trees and to increase soil moisture via capillary water rise (Dislich et al., 2016). This compaction practice is expected to depress peat oxidative decomposition due to the increase in soil water content and decrease in soil gas diffusivity (Melling et al., 2005, 2013a).

It has been reported that CO_2 emissions from tropical drained peatland are an important part of the global C cycle (Sjögersten et al., 2014; Miettinen et al., 2017), and therefore it is important to quantify oxidative peat decomposition or heterotrophic respiration (R_H) from total soil respiration (R_S) separately. However, there have been few

82 studies of R_H in tropical peatland, despite R_H being an important component of R_S that
83 corresponds to oxidative peat decomposition. For oil palm plantations on peat, some
84 studies have measured R_H periodically at intervals of one or more months for periods
85 equal to or less than 1 year (Melling et al., 2005, 2013a, 2013b; Dariah et al., 2014;
86 Husnain et al., 2014; Marwanto and Agus, 2014; Sakata et al., 2015; Comeau et al., 2016).
87 Due to the limitations of field studies, the controlling factors of soil CO_2 efflux are not
88 well understood at the process level. For example, it was reported that no significant
89 relationship exists between R_S and groundwater level (GWL) (Jauhiainen et al., 2008),
90 probably due to the disconnection of capillary force under dry conditions, resulting in soil
91 moisture in the topsoil becoming decoupled from the GWL (Ishikura et al., 2017). Soil
92 moisture in the topsoil can be a better predictor than GWL for soil CO_2 efflux (Melling
93 et al., 2005, 2013a), because soil moisture is affected more by capillary rise than GWL
94 when a peat soil is compacted (Price, 1997; Michel et al., 2001). However, the
95 relationship between soil CO_2 efflux and soil moisture in tropical peat ecosystems is still
96 not well understood. For a better understanding, long-term continuous measurement of
97 both R_S and R_H is necessary to capture diurnal variation, detect the response of soil CO_2
98 efflux to dynamic environmental variations, and reduce the uncertainties in assessment
99 of annual CO_2 emissions. To our knowledge, no studies have measured R_S and R_H
100 continuously in an oil palm plantation on peat.
101 Oxidative peat decomposition induces subsidence together with physical consolidation
102 and shrinkage (Stephens and Stewart, 1976; Wösten et al., 1997; Hooijer et al., 2012). If
103 the contribution of peat oxidation to total subsidence is determined, CO_2 emissions
104 through peat decomposition can be estimated from subsidence monitoring (Couwenberg
105 and Hooijer, 2013). However, the extent of this contribution has not yet been determined,

because it depends on peat conditions, such as GWL and the time since drainage. Field studies involving simultaneous measurement of peat subsidence and oxidative peat decomposition could enable this to be determined, but only a few studies have been reported (Wakhid et al., 2017).

Therefore, R_S and R_H due to oxidative peat decomposition were measured continuously for two years using an automated chamber system, together with GWL, soil moisture, and peat subsidence in an oil palm plantation established on tropical peat. The objectives of this study were to investigate seasonal changes in R_S and R_H in relation to soil water conditions, quantify annual cumulative R_S and R_H values, and evaluate the contribution of oxidative peat decomposition to subsidence.

2. Material and methods

2.1 Site description

This study was conducted in an oil palm (*Elaeis guineensis* Jacqu.) plantation (2°11'N, 111°50'E) in a watershed of the Rajang River in Sibu, Sarawak, Malaysia (Fig. 1) at an elevation of approximately 25 m above sea level. The mean annual air temperature and precipitation between 2004 and 2016 were 26.5 ± 0.2°C and 2,915 ± 213 mm yr^{-1} (mean ± 1 standard deviation (SD)), respectively, at the Sungai Salim B meteorological station (Department of Irrigation and Drainage Malaysia), which is 7.4 km from the study site. In September 2004, a mixed peat swamp forest on an ombrotrophic peat dome was converted to an oil palm plantation, with the installation of ditches and water gates; artificial compaction to prevent palms from leaning and toppling was performed during land preparation. The soil type was a Sapric Histosol (IUSS Working Group WRB, 2015), with a peat depth of 12.7 m. Palm seedlings were planted on a triangular grid spacing of

8.5 m between trees (153 trees ha^{-1}; Fig. 2), and the ground was sparsely covered by fern plants (*Stenochlaena palustris* (Burm. f.) Bedd.). The lower fronds of oil palm trees were periodically lopped and piled in inter-row spaces. Thus, little leaf litter accumulated on the ground, except for some areas with fern plants. In 2014, the palm trees were 9 years old, and the canopy height was about 8 m. Oil palm plantations are commonly replanted every 25–30 years (Basiron, 2007), so the study site was in the first cycle of cultivation. The following fertilizers were applied together four times a year (January, March, July–August, and September–October) within 1 m of each stem: 74–147 kg N ha^{-1} yr^{-1} of urea, 7–9 kg P ha^{-1} yr^{-1} of rock phosphate, and 239–311 kg K ha^{-1} yr^{-1} of muriate of potash (KCl). Copper, zinc, and boron were applied as micronutrients at 8–16 kg ha^{-1} yr^{-1} in May–June every year, and kieserite ($MgSO_4 \cdot H_2O$) was also applied at rates of 80 kg ha^{-1} in October 2014, 119 kg ha^{-1} in May 2015, and 80 kg ha^{-1} in January 2016, respectively.

2.2 Experimental design and chamber measurement

In April 2014, an experimental area without fern plants was established, and the following treatments were applied (Fig. 2):

Close-to-tree (CT, four plots): distance from the nearest tree < 2.5 m, corresponding to R_S.

Far-from-tree (FT, four plots): distance from the nearest tree > 3 m, corresponding to R_S.

Root-cut (RC, four plots): distance from the nearest tree > 3 m with trenching, corresponding to R_H.

In each RC plot, four stainless steel plates were inserted surrounding an area of 40 × 80 cm^2. The depth of insertion was 80 cm, which was almost equivalent to the lowest GWL. In May 2014, 1 month later, an automated chamber system was installed in the

154 experimental area. The system consisted of 16 chambers, an infrared CO_2 analyzer (LI-
155 820, LI-COR, Inc., Lincoln, Nebraska, USA), a programmable data logger (CR1000,
156 Campbell Scientific Inc., Logan, Utah, USA), and an air pump and solenoid valves
157 (Hirano et al., 2009). The chamber consisted of an opaque polyvinyl chloride (PVC)
158 cylinder (height: 40 cm; inner diameter: 25 cm). Chambers were inserted 2–3 cm deep
159 into the soil. One chamber was installed in each CT and FT plot, and two chambers were
160 installed in each RC plot (Fig. 2).

161 An opaque PVC lid was attached to the chamber top that opened vertically and closed
162 under the control of the data logger. Each chamber closed for 225 s in sequence, one after
163 the other, and it took 1 h for all chambers to close/open in rotation. The air in the
164 headspace of each chamber was circulated through the CO_2 analyzer when the chambers
165 were closed. The CO_2 concentration was measured at 10-s intervals and recorded in the
166 data logger. In August 2015, a greenhouse gas analyzer (Ultraportable Greenhouse Gas
167 Analyzer 915-0011, Los Gatos Research, Inc., San Jose, California, USA) was placed in
168 the air circulation line to measure CO_2, methane, and water vapor concentrations.
169 Although measurements began in May 2014, data for a two-year period from January
170 2015 were used, because additional CO_2 emissions resulting from the decomposition of
171 dead roots left in the trenched plots were expected to occur for several months after
172 trenching (Hanson et al., 2000; Comeau et al., 2016). One palm tree fell on a chamber in
173 a CT plot in August 2015, and the chamber was then moved to an FT position. Thus, the
174 number of CT plots decreased to three, while the number of FT plots increased to five in
175 2016. CO_2 data from the CO_2 analyzer were primarily used; data from the greenhouse gas
176 analyzer were used as an alternative when the LI-820 malfunctioned. During the two
177 years of 2015 and 2016, 23% of the data was lost, mainly due to power problems.

Soil CO_2 efflux was calculated from the increase in CO_2 concentration in the chamber headspace during the 90–220 s after the chamber closing:

$$F = \frac{PH}{RT_{\text{air}}}\frac{dC}{dt} \quad (1)$$

where F is soil CO_2 efflux (μmol m^{-2} s^{-1}), P is air pressure (101.325 kPa), H is the aboveground height of a chamber, R is the gas constant (8.314 Pa m^3 K^{-1} mol^{-1}), T_{air} is air temperature (K), and dC/dt is the rate of increase of the CO_2 concentration (μmol mol^{-1} s^{-1}). The quality of soil CO_2 efflux data was controlled as follows:

1. Significant slope: the Pearson's correlation coefficient for the rate of increase in the CO_2 concentration should be higher than 0.661376 ($P < 0.01$, $n = 14$);
2. Stationary slope: the rates of increase in CO_2 concentration from 90–150 s and from 160–220 s after closing were calculated separately. The difference between the means of the two rates and the rate during the whole period (90–220 s) should be less than 30% (Aguilos et al., 2013);
3. Outliers: the CO_2 flux should be within 0–40 μmol m^{-2} s^{-1}.

After these quality control criteria were applied, 43% of the data remained available. Because no litter accumulated in any chamber, CO_2 emissions resulting from leaf litter decomposition were not included in either R_S or R_H in this study. The CO_2 fluxes measured by the two CO_2 analyzers did not differ significantly from each other (Fig. S1).

2.3 Environmental properties

Precipitation was observed at a height of 1 m in an open space about 5 m away from the experimental area. However, some data were lost due to power problems, and precipitation data from the Sungai Salim B meteorological station were therefore used to record annual precipitation. The friction velocity (u^*, m s^{-1}) was measured at a height of

21 m above the vegetation canopy using a sonic anemometer (CSAT3, Campbell Scientific Inc.) and was used as an index of atmospheric turbulence.

Air and soil temperatures (°C) at a depth of 5 cm were measured using thermocouple thermometers in the same two chambers in FT plots. The GWL (m, negative values represent belowground) was measured using a piezometer (HTV-050KP, Sensez, Tokyo, Japan) at one point (Fig. 2), and volumetric soil water content ($m^3\ m^{-3}$) at 0–30-cm depth was measured using a time-domain reflectometry (TDR) sensor (CS616, Campbell Scientific Inc.) in FT and RC plots, respectively (Fig. 2). Half-hourly means of these belowground variables were also recorded to the data logger used for the chamber system. Missing daily mean GWLs were gap-filled by a tank model (He and Inoue, 2015). The water retention curve was fitted to the relationship between daily mean GWL and soil water content using van Genuchten's model (van Genuchten, 1980):

$$\theta = \theta_{\mathrm{res}} + \frac{\theta_{\mathrm{sat}} - \theta_{\mathrm{res}}}{(1 + (\alpha h)^n)^{1-1/n}} \quad (2)$$

where θ is the soil water content, θ_{sat} is the saturated soil water content (equivalent to the porosity explained below), h is the pressure head (= −100 × GWL, cm), and α, n, and θ_{res} are fitting parameters, respectively. Missing daily mean soil water contents were gap-filled from the GWL using the water retention curve (Fig. S3).

In June 2014, six undisturbed soil cores of 100 cm^3 were taken to a depth of 60 cm at intervals of 10 cm using a stainless soil core cylinder. Bulk density ($Mg\ m^{-3}$) and porosity ($m^3\ m^{-3}$) were determined using a digital soil volume analyzer (DIK-1110, Daiki Rika Company, Saitama, Japan). A further three disturbed soil samples were taken to a depth of 60 cm at intervals of 10 cm, and the total C and nitrogen (N) contents (%) were analyzed by the dry combustion method (TruMac CN, LECO Corporation, St. Joseph,

Michigan, USA). Other undisturbed soil cores of 100 cm^3 were taken from depths of 0–5, 5–10, 10–20, and 20–30 cm every month during the study period, and the volumetric soil water content was determined using the digital soil volume analyzer. Volumetric soil water content measured by the TDR sensor was calibrated using the soil water content measured by the soil core method. Water-filled pore space (WFPS, m^3 m^{-3}) was calculated from the proportion of soil water content to soil porosity.

In February 2017, disturbed topsoil at a depth of 0–30 cm was sampled in four replicate locations around the experimental area. Soil pH (1:2.5 H_2O) was measured using a digital pH meter (827 pH Lab, Metrohm AG, Herisau, Switzerland). Ash content (%) was analyzed by loss-on-ignition (TGA701, LECO Corporation) at 800°C for more than 1 h. To measure fine root biomass (diameter: <2 mm), 100 cm^3 soil cores were taken at a depth of 0–10 cm at 1, 2, and 3 m from the four nearest palm trees, respectively. The soil samples were washed and sieved through a 2-mm mesh. Living fine roots were picked out by visual assessment and elasticity, and dried at 75°C for more than 48 h to measure biomass.

2.4 Subsidence and the contribution of peat decomposition

In May 2014, a subsidence pole with a marking disk was installed vertically into the soil until it reached the mineral soil beneath the peat. Because the measurement height of the pole from the ground surface was affected by the roughness of the ground, the marking disk was used to take an average. The disk could move freely along the anchored pole, and thus was always resting on the ground surface. The heights from the disk on the ground to the top of the pole were measured manually on four sides and averaged every month from June 2014. Annual subsidence was calculated as the cumulative subsidence from January in one year to January in the following year.

Subsidence through oxidative peat decomposition (S_{RH}, cm $period^{-1}$) was calculated

using the following equation (Wakhid et al., 2017):

$$S_{\mathrm{RH}} = \frac{\text{Cumulative } R_{\mathrm{H}}}{10 \cdot \mathrm{BD} \cdot \mathrm{TC}} \quad (3)$$

where cumulative R_{H} (kg C m^{-2} $period^{-1}$) is the cumulative CO_2 emission in RC plots, BD (Mg m^{-3}) is bulk density, and TC (g C g^{-1}) is the total C content of the soil.

2.5 Data analysis

Nonlinear mixed-effects modeling was applied to analyze the dependencies of the daily mean soil CO_2 efflux (μmol m^{-2} s^{-1}) on GWL (m) and WFPS (m^3 m^{-3}) for each of the CT, FT, and RC plots by fitting the following equations:

$$\mathrm{CO_2\ efflux} = R_0 \cdot \exp(b \cdot \mathrm{GWL}) \quad (4)$$

$$\mathrm{CO_2\ efflux} = R_0 \cdot \exp\big(b \cdot (1 - \mathrm{WFPS})\big) \quad (5)$$

where R_0 and b are regression coefficients, and chambers are treated as the random coefficients of R_0 and b. The residual maximum likelihood (REML) estimation method was used for regression analysis, and the goodness-of-fit was evaluated by the coefficient of determination (R^2).

The daily mean soil CO_2 efflux was gap-filled from the daily mean GWL or WFPS using a regression equation [Eqs. (4) or (5)], and annual cumulative CO_2 emissions were summed for each chamber. The differences in the means of the annual cumulative CO_2 emissions among years (2015 and 2016) and treatments (CT, FT, and RC plots) were tested by a two-way analysis of variance (ANOVA) and a multiple comparison using the Tukey–Kramer method. The ratios of R_{H} to R_{S} were calculated by dividing the annual soil CO_2 emissions of RC plot by those of CT and FT plots.

Subsidence through the physical processes of shrinkage/swelling and consolidation

(cm period^{-1}) was determined monthly as the difference between total subsidence and S_{RH}. It was assumed that physical subsidence (S_{phys}) progressed logarithmically over time due to secondary consolidation and fluctuated with GWL by shrinkage/swelling [Eq. (6)]. In this simple model, C leaching, especially dissolved organic carbon (DOC) efflux through groundwater discharge (Moore et al., 2011), was incorporated into the first term on the right side. However, the regression of cumulative subsidence over time can be spurious, because cumulative subsidence is probably a unit root process. Therefore, a unit root test (augmented Dickey–Fuller test) was performed for S_{phys}. As a result, S_{phys} was significantly stationary ($P < 0.05$) so a linear regression was performed using the following equation:

$$S_{phys} = a \cdot \log_{10}(\text{Days}) + b \cdot (\text{GWL}_i - \text{GWL}_0) \quad (6)$$

where the term Days is the number of days from the beginning of subsidence measurement (June 23, 2014), GWL_0 is the daily mean GWL on the initial date (= −0.73 m), GWL_i is the daily mean GWL when subsidence was measured, and a and b are regression coefficients. Because soil CO_2 efflux was available only from January 2015, S_{RH} in 2014 was estimated from the GWL using Eq. (4). Finally, the smoothed annual total subsidence (S_{sm}, cm yr^{-1}) was calculated using the following equation:

$$S_{sm} = a \cdot \log_{10}\left(\frac{\text{Days}_{y+1}}{\text{Days}_y}\right) + b \cdot \left(\overline{\text{GWL}_y} - \text{GWL}_0\right) + S_{RH\,y} \quad (7)$$

where y is the target year (2015 or 2016), Days_y is the number of days after January 1 in y since the beginning of subsidence measurement (June 23, 2014), $\overline{\text{GWL}_y}$ is the annual

mean GWL in y, and annual $S_{RH\,y}$ is subsidence through R_H in y.

All data analyses were conducted using R software (R Core Team, 2017).

3. Results

3.1 Environmental properties

The soil pH was 3.9 ± 1.0 (mean ± 1 SD) and the soil C content was 52.8 ± 0.8%; such a low pH and high C content are typical properties of ombrotrophic peat. Bulk density was 0.16 ± 0.04 Mg m^{-3} at a depth of 0–10 cm and 0.12 ± 0.02 Mg m^{-3} at a depth of 0–60 cm (Table S1). The ash content was relatively high at 7.1 ± 7.9% because of fertilizer applications. Fine root biomass values were 165 ± 91, 86 ± 63, and 93 ± 25 g m^{-2} at a depth of 0–10 cm at 1, 2, and 3 m from the nearest tree, respectively.

Annual precipitation amounts in 2015 and 2016 were similar and close to the mean annual precipitation recorded over a 13-year period (2,915 mm yr^{-1}) (Fig. 3a, Table 1). Daily mean GWL varied from −0.89 to −0.23 m (Fig. S2), with similar annual means in 2015 and 2016 (Fig. 3b, Table 1). The WFPS did not change between 2015 and 2016 (Table 1) and values were similar in the RC and FT plots. No significant difference was found in daily mean soil temperatures between 2015 and 2016 (Table 1).

3.2 Diurnal changes in soil carbon dioxide efflux

Soil temperature at a depth of 5 cm displayed a typical diurnal pattern with a minimum at 7 h and a maximum at 14 h. The diurnal range was about 10ºC (Fig. 4a). Soil temperature was higher than air temperature in the nighttime by about 2ºC on average (Fig. 4a). The u^* was higher in the daytime than in the nighttime (Fig. 4a). In contrast, soil CO_2 efflux was higher in the nighttime than in the daytime in all treatments (Fig. 4b). Its diurnal pattern was a mirror image of those of temperature and u^*.

311 To examine the effects of temperature, soil water condition, and u^* on diurnal changes
312 in soil CO_2 efflux, a multiple regression was performed for hourly soil CO_2 efflux with
313 soil temperature, GWL, the difference between air and soil temperature ($\Delta T_{air\text{-}soil}$, defined
314 as air temperature minus soil temperature), and u^* as predictors (Table 2). Soil
315 temperature was a significant predictor only in RC plots, while GWL, $\Delta T_{air\text{-}soil}$, and u^*
316 were significant predictors in all treatments. From their standardized regression
317 coefficients, $\Delta T_{air\text{-}soil}$ was the strongest predictor followed by u^*, with no general diurnal
318 change expected in GWL. Hourly soil CO_2 efflux was plotted against $\Delta T_{air\text{-}soil}$ and u^*,
319 respectively (Fig. 5). Soil CO_2 efflux had a significant negative relationship with $\Delta T_{air\text{-}soil}$
320 in each treatment when $\Delta T_{air\text{-}soil}$ was negative (Fig. 5a). A significant negative relationship
321 was found between soil CO_2 efflux and u^* in each treatment when u^* was lower than
322 around 0.4 m s^{-1} (Fig. 5b).

323 **3.3 Seasonal changes in soil carbon dioxide efflux**

324 To remove bias due to diurnal changes, the daily mean soil CO_2 efflux was calculated
325 only when the number of available data points was larger than six in both the daytime (7–
326 18 h) and nighttime (19–6 h), respectively. The daily mean soil CO_2 efflux values during
327 the two years were 2.80 ± 2.18, 1.59 ± 1.18, and 1.94 ± 1.58 μmol m^{-2} s^{-1} (mean ± 1 SD)
328 in the CT, FT, and RC plots, respectively (Fig. 6). Nonlinear mixed-effects models using
329 GWL and WFPS [Eqs. (4) and (5), respectively] were significantly fitted ($P < 0.001$) to
330 daily mean soil CO_2 efflux (Fig. 7). It was found that the daily mean soil CO_2 efflux
331 increased significantly as the GWL or WFPS decreased. The regression with GWL
332 produced higher R^2 values than that with WFPS in the CT and FT plots, while the
333 regression with WFPS produced slightly higher R^2 values than the regression with GWL
334 in RC plots (Fig. 7).

3.4 Annual cumulative soil carbon dioxide emission

The daily mean soil CO_2 flux was gap-filled from the GWL using the model [Eq. (4), Fig. 7], and annual sums were calculated (Table 3). Annual cumulative soil CO_2 emissions did not differ between 2015 and 2016 ($F_{1, 27} = 1.59$, $P = 0.22$), but differed significantly among the CT, FT, and RC plots ($F_{2, 27} = 4.05$, $P < 0.05$). The highest soil CO_2 emission was measured in the CT plots (1.03 ± 0.53 kg C m^{-2} yr^{-1}), and the lowest was measured in the FT plots (0.59 ± 0.26 kg C m^{-2} yr^{-1}). The R_H/R_S ratios were 0.66 and 1.16 for RC/CT and RC/FT, respectively (Table 3).

3.5 Subsidence

The ground surface subsided, but oscillated in correspondence with the GWL (Fig. 8). Total annual subsidence values were determined instantaneously from two measurements in January to be 1.23 and 2.02 cm yr^{-1} in 2015 and 2016, respectively (Table 4). The annual S_{RH} was calculated from the annual R_H, the bulk density, and C content of 60-cm-thick surface peat using Eq. (3). The result shows that the oxidative subsidence values were 1.22 and 0.99 cm yr^{-1} in 2015 and 2016, respectively (Table 4). As a result, the contributions of oxidative peat decomposition to total subsidence were 100 and 49% in 2015 and 2016, respectively, with a mean of 74%.

Physical subsidence (S_{phys}) was significantly fitted with Eq. (6) as $S_{phys} = 1.42 \cdot \log_{10}(\text{Days}) - 6.46 \cdot (\text{GWL}_i + 0.73)$ ($P < 0.01$). The result indicated that the ground subsided physically by 0.65 cm for every GWL lowering of 10 cm. Annual smoothed subsidence (S_{sm}) values were 1.83 and 1.27 cm yr^{-1}, respectively, in 2015 and 2016. The S_{RH} accounted for 67 and 78% of the smoothed subsidence in 2015 and 2016, respectively, with a mean of 72% (Table 4).

4. Discussion

4.1 Factors controlling soil carbon dioxide efflux

Soil CO_2 efflux displayed a clear diurnal pattern that was almost in reverse parallel with soil temperature (Fig. 4). The hourly soil CO_2 efflux had significant negative relationships with GWL, $\Delta T_{\text{air-soil}}$, and u^* (Table 1). First, the effects of $\Delta T_{\text{air-soil}}$ and u^* on the diurnal change in soil CO_2 efflux are considered.

Soil temperature was higher than air temperature at night (Fig. 4a), and soil CO_2 efflux increased significantly as $\Delta T_{\text{air-soil}}$ decreased when $\Delta T_{\text{air-soil}}$ was negative (Table 2, Fig. 5a). Ganot et al. (2014) found that soil CO_2 efflux was promoted by the upward mass flow due to thermal convection in porous mineral soils when the soil temperature was higher than the air temperature. In this study, unsaturated peat soil was more porous than mineral soil. Therefore, our results imply that soil CO_2 efflux was promoted by thermal convection in the unsaturated peat profile. Furthermore, the nighttime thermal convection probably decreased soil CO_2 concentrations more than diffusion, which potentially suppressed soil CO_2 efflux during the following daytime period under stable thermal conditions. On the other hand, Lai et al. (2012) reported that soil CO_2 flux was underestimated by the closed chamber method during periods with a high u^* in boreal peatland because wind pumps out the soil air just below the ground surface, which decreases the soil CO_2 concentration. The chamber method can measure only the diffusive CO_2 efflux in the closed space, but cannot measure the CO_2 mass flow due to atmospheric turbulence. In this study, the hourly soil CO_2 efflux decreased significantly as u^* increased (Fig. 5b), which may have led to an underestimation of soil CO_2 efflux in the daytime when u^* was high on average (Fig. 4a). Therefore, the diurnal change probably resulted from the combination of an increased flux in the nighttime due to

383 thermal convection, a decreased flux in the daytime due to the aftereffect of nighttime
384 thermal convection, and an underestimated flux in the daytime due to pumping by
385 atmospheric turbulence. In the calculation of the daily soil CO_2 efflux, the positive and
386 negative effects of thermal convection can be compensated for by making continuous
387 measurements, although some underestimation due to mass flow through pumping is
388 inevitable in a porous soil when the chamber method is applied, especially in unsaturated
389 peat soils.

390 Soil CO_2 flux increases with soil temperature. The diurnal changes in soil temperature
391 at a depth of 5 cm, with a diurnal range of about 5ºC (Fig. 4a), could have had a positive
392 effect on soil CO_2 efflux. However, the effect of soil temperature was not significant in
393 the CT and FT plots (Table 2). The effect of soil temperature was weaker than that of the
394 other environmental properties in the RC plots, although it was significant due to the large
395 sample size (Table 2). Oxidative peat decomposition would have occurred within the 60-
396 cm deep unsaturated peat horizon because the annual mean GWL was about −0.6 m
397 (Table 1). Thus, soil CO_2 efflux resulting from the total peat decomposition was not
398 directly related to soil temperature, which was similar to the oxidative peat decomposition
399 observed in a burnt ex-peat swamp forest in Central Kalimantan, Indonesia (Hirano et al.,
400 2014).

401 The effects of GWL and WFPS on the daily mean soil CO_2 efflux were then considered.
402 The soil CO_2 flux had a negative exponential relationship with the GWL in all treatments
403 (Fig. 7), which indicates that soil CO_2 efflux was promoted by lowering of the GWL. A
404 negative relationship between soil CO_2 efflux and GWL has been reported in various
405 tropical peatlands (Furukawa et al., 2005; Hirano et al., 2009, 2014; Couwenberg et al.,
406 2010; Sundari et al., 2012; Ishikura et al., 2017), indicating that peat decomposition is

promoted by lowering of the GWL. Lowering of the GWL decreases WFPS and enhances aeration of the soil. As a result, oxidative mineralization of organic matter and gas diffusivity in the soil is accelerated, resulting in increased soil CO_2 efflux (Linn and Doran, 1984). The relationship between soil CO_2 efflux and WFPS in the 30-cm-thick surface peat was also significant, but was weaker than the relationship with GWL in the CT and FT plots, while the relationships were similar in the RC plots (Fig. 7). In contrast, Ishikura et al. (2017) suggested that WFPS might be better able to explain the variation in peat soil CO_2 efflux than GWL in Central Kalimantan, Indonesia, because disconnection of the capillary force between surface soil water and groundwater occurred under dry conditions. However, at the site used in the current study, such a disconnection probably did not occur (Fig. S3) because GWL was controlled by water gates and remained relatively high. Melling et al. (2013a) found that WFPS was a better predictor of soil CO_2 efflux than was GWL over a WFPS range of 0.6–0.9 m^3 m^{-3}. However, in the current study the range was narrower (0.60–0.75 m^3 m^{-3}), although the GWLs were similar between this study and that of Melling et al. (2013a). The bulk density in Melling et al. (2013a) was higher (0.21–0.23 Mg m^{-3}) than that recorded in this study (Table 4, S1). Therefore, the effect of a capillary rise on WFPS might have been higher in Melling et al. (2013a) than in this study due to the higher bulk density and lower porosity. These are reasons why WFPS was not a better predictor than GWL in this study.

4.2 Annual cumulative carbon dioxide emission

In this study, 57% of the data from continuous CO_2 flux measurements during the two years was lost due to power problems and quality controls. To calculate annual cumulative CO_2 emissions, the data gaps were filled on a daily basis from GWL using negative exponential equations (Fig. 7). Although gap filling causes uncertainties in the assessment

431 of annual emissions, these uncertainties are limited because the seasonal variation in
432 GWL was not large at this study site (Fig. 3b, S2). The annual values are expected to be
433 more reliable than those reported in previous studies, because previous studies estimated
434 annual values from data collected at intervals of one month or longer.

435 Annual soil CO_2 emission was significantly larger from the CT plots than from the RC
436 plots, and R_H accounted for 66% of R_S (Table 3). In contrast, the annual soil CO_2 emission
437 from the FT plots did not differ significantly from that of the RC plots (Table 3). Dariah
438 et al. (2014) measured soil CO_2 efflux at different distances from tree stems in an oil palm
439 plantation on tropical peat and reported that root respiration was negligible at distances
440 of more than 3 m. The distance of each FT plot from the nearest palm tree was greater
441 than 3 m. Thus, the soil CO_2 efflux in the FT plots was mostly derived from R_H, and root
442 respiration was probably negligible.

443 The Intergovernmental Panel on Climate Change (IPCC, 2014) provides a default CO_2
444 emission factor of 1.1 kg C m^{-2} yr^{-1}, with 95% confidence intervals of 0.56–1.7 kg C m^{-2}
445 yr^{-1}, from tropical peat in oil palm plantations for their Tier 1 methodology, although this
446 value was derived from results obtained by the closed chamber and subsidence methods.
447 The annual R_H measured in the RC plots was almost equivalent to the bottom 95%
448 confidence interval of the Tier 1 method. The annual R_S in the CT plots was lower than
449 the range of 1.22–1.81 kg C m^{-2} yr^{-1} reported in previous studies conducted in oil palm
450 plantations on peat (Melling et al., 2005, 2013b; Dariah et al., 2014; Sakata et al., 2015).
451 The annual R_H was lower than the previously reported range of 0.69–1.80 kg C m^{-2} yr^{-1}
452 (Melling et al., 2013b; Dariah et al., 2014; Husnain et al., 2014; Marwanto and Agus,
453 2014). The low R_S and R_H in this study may have been caused by the higher annual mean
454 GWL (−1.24 to −0.58 m) than reported in previous studies (Table 1) and by the exclusion

455 of leaf litter decomposition. In addition, previous studies calculated annual soil CO_2
456 emissions either by linear interpolation of the monthly CO_2 flux (Melling et al., 2005,
457 2013b; Sakata et al., 2015) or by simply averaging periodic CO_2 flux measurements for
458 less than 1 year (Dariah et al., 2014; Husnain et al., 2014; Marwanto and Agus, 2014),
459 whereas in this study annual CO_2 emissions were calculated from the quality controlled
460 continuous flux, and data gaps were filled using continuous GWL data. The difference in
461 the calculation methods used would also affect the reported annual soil CO_2 emissions.
462 The contribution of oxidative peat decomposition to total soil respiration calculated as
463 RC/CT (Table 3) was comparable with the range of 60–86% reported in other oil palm
464 plantations on tropical peat (Dariah et al., 2014; Comeau et al., 2016), except for 38% in
465 Melling et al. (2013).

466 When considering other land uses on tropical peat, the R_S in this study was lower than
467 the values of 1.23 and 1.35 kg C m^{-2} yr^{-1} reported in swamp forests (Sundari et al., 2012),
468 1.68–4.20 kg C m^{-2} yr^{-1} reported in an *Acacia* plantation (Jauhiainen et al., 2012), 3.29
469 kg C m^{-2} yr^{-1} reported in a rubber plantation (Wakhid et al., 2017), and 1.11–1.60 kg C
470 m^{-2} yr^{-1} reported in a sago palm plantation (Melling et al., 2005, 2013b). The R_H in this
471 study was also lower than the ranges of 0.70–0.83 kg C m^{-2} yr^{-1} reported in swamp forests
472 (Itoh et al., 2017), 1.91–3.78 kg C m^{-2} yr^{-1} reported in an *Acacia* plantation (Jauhiainen
473 et al., 2012), and the value of 1.41 kg C m^{-2} yr^{-1} reported in a rubber plantation (Wakhid
474 et al., 2017), while it was similar to the range of 0.60–0.76 kg C m^{-2} yr^{-1} reported in sago
475 palm plantations (Melling et al., 2005, 2013b; Watanabe et al., 2009). In *Acacia*
476 plantations, GWL tends to be lower than in oil palm plantations (Hergoualc'h and Verchot,
477 2011), which would enhance oxidative peat decomposition.

4.3 Subsidence

The annual total subsidence that was determined instantaneously was higher in 2016 than in 2015, whereas the annual smoothed subsidence was higher in 2015 (Table 4); the interannual difference was larger for instantaneous subsidence. Instantaneous subsidence was calculated simply from two measurements at annual intervals, and therefore was dependent on peat surface oscillation due to short-term variations in GWL. Therefore, the smaller instantaneous subsidence in 2015 was caused by the higher GWL in January 2016 (Fig. 8). In addition, the interannual order of instantaneous subsidence (2015 < 2016) was inconsistent with that of annual R_H (2015 > 2016) (Table 4). Because such surface oscillation due to short-term GWL variation was excluded in the smoothed subsidence, annual values reflected the interannual variation in GWL (Table 1) and their order of magnitude was consistent with that of the annual R_H (2015 > 2016). However, the means of annual subsidence for the two years were similar in the two approaches.

The annual total subsidence in this study (Table 4) was lower than the range of 2.0–5.4 cm yr^{-1} reported in previous studies of oil palm plantations on peat (Wösten et al., 1997; Hooijer et al., 2012; Couwenberg and Hooijer, 2013), and was also lower than the 5 cm yr^{-1} in an *Acacia* plantation (Hooijer et al., 2012) and 5.96 cm yr^{-1} in a rubber plantation (Wakhid et al., 2017) on tropical peat. These studies reported a higher oxidative peat decomposition of 0.69–2.13 kg C m^{-2} yr^{-1} than was found in this study, which probably resulted in higher subsidence. Previous studies in tropical peatland also reported a lower bulk density of 0.12–0.14 Mg m^{-3} than was found in this study, except for the value of 0.24 Mg m^{-3} reported by Wakhid et al. (2017). Subsidence increases bulk density, and an increased bulk density decreases subsidence (van Asselen, 2011). Thus, the lower subsidence reported in this study was probably attributable to the higher bulk density due

to peat compaction during land preparation before planting.

Peat oxidation accounted for 72 to 74% of total subsidence on an annual basis (Table 4), which was almost in the middle of the 50–92% range reported in previous studies conducted in tropical peatlands (Murayama and Bakar, 1996; Wösten et al., 1997; Hooijer et al., 2012), except for the value of 25% reported in a rubber plantation (Wakhid et al., 2017).

5. Conclusions

Soil CO_2 efflux through both soil respiration and oxidative peat decomposition were measured continuously for two years in an oil palm plantation established on tropical peat. From the large amount of continuous data, it was found that soil CO_2 efflux was lower in the daytime. The opposite diurnal variation for soil and air temperatures was attributable to the mass flow of soil air due to thermal convection at night and to atmospheric turbulence in the daytime. This indicates that periodic measurements conducted only in the daytime would lead to underestimation of soil CO_2 efflux. In addition, further studies are necessary to determine the reliability of chamber methods on peat, which is one of the most porous soils.

The environmental controls on soil CO_2 efflux using daily means were analyzed to exclude diurnal variation in CO_2 efflux. As a result, exponential negative relationships were found between soil CO_2 efflux and GWL even under a relatively narrow seasonal variation in GWL due to water management. Annual gap-filled CO_2 emissions through soil respiration and oxidative peat decomposition were both lower than those in other oil palm plantations on tropical peat, possibly due to the higher GWL and peat compaction observed in this study compared to previous studies. Thus, water management to raise the

GWL is important to mitigate soil CO_2 emissions from oil palm plantations on tropical peat. The differences among studies could also be due to differences in precipitation patterns, land-use history, or other factors among plantations. Therefore, further field studies are necessary to reduce the uncertainties in the emission factor of CO_2 from oil palm plantations in Southeast Asia's tropical peatland.

Acknowledgements

The authors would like to thank the staff of Sarawak Tropical Peat Research Institute for their support during the study and Shun-ichi Nakatsubo at the Institute of Low Temperature Science, Hokkaido University for chamber preparation. Malaysian Meteorological Department (Sarawak branch) and Department of Irrigation and Drainage, Sarawak supported us to provide the meteorological data for this study. This study was supported by the Sarawak State Government and Federal Government of Malaysia. This study was conducted under the Joint Research Program of the Institute of Low Temperature Science, Hokkaido University, and was also supported by the Japan Society for the Promotion of Science (JSPS) KAKENHI (no. 25257401), the Environment Research and Technology Development Fund (no. 2-1504) of the Environmental Restoration and Conservation Agency and the Ministry of the Environment, Japan, the Asahi Glass Foundation, and a Grant for Environmental Research Projects from The Sumitomo Foundation.

548 **References**

549 Aguilos, M., Takagi, K., Liang, N., Watanabe, Y., Teramoto, M., Goto, S., Takahashi,
550 Y., Mukai, H., Sasa, K., 2013. Sustained large stimulation of soil heterotrophic
551 respiration rate and its temperature sensitivity by soil warming in a cool-temperate
552 forested peatland. Tellus 65B, 1–13.
553 Basiron, Y., 2007. Palm oil production through sustainable plantations. Eur. J. Lipid
554 Sci. Technol. 109, 289–295.
555 Comeau, L.-P., Hergoualc, K., Hartill, J., Smith, J., Verchot, L. V., Peak, D.,
556 Mohammad, A., 2016. How do the heterotrophic and the total soil respiration of an
557 oil palm plantation on peat respond to nitrogen fertilizer application? Geoderma
558 268, 41–51.
559 Couwenberg, J., Dommain, R., Joosten, H., 2010. Greenhouse gas fluxes from tropical
560 peatlands in south-east Asia. Glob. Chang. Biol. 16, 1715–1732.
561 Couwenberg, J., Hooijer, A., 2013. Towards robust subsidence-based soil carbon
562 emission factors for peat soils in south-east Asia, with special reference to oil palm
563 plantations. Mires Peat 12, 1–13.
564 Dariah, A., Marwanto, S., Agus, F., 2014. Root- and peat-based CO_2 emissions from oil
565 palm plantations. Mitig. Adapt. Strateg. Glob. Chang. 19, 831–843.
566 Dislich, C., Keyel, A.C., Salecker, J., Kisel, Y., Meyer, K.M., Auliya, M., Barnes, A.D.,
567 Corre, M.D., Darras, K., Faust, H., Hess, B., Klasen, S., Knohl, A., Kreft, H.,
568 Meijide, A., Nurdiansyah, F., Otten, F., Pe'er, G., Steinebach, S., Tarigan, S.,
569 Tölle, M.H., Tscharntke, T., Wiegand, K., 2016. A review of the ecosystem
570 functions in oil palm plantations, using forests as a reference system. Biol. Rev. 49,
571 doi: 10.1111/brv.12295.

572 Furukawa, Y., Inubushi, K., Ali, M., Itang, A.M., Tsuruta, H., 2005. Effect of changing
573 groundwater levels caused by land-use changes on greenhouse gas fluxes from
574 tropical peat lands. Nutr. Cycl. Agroecosystems 71, 81–91.
575 Ganot, Y., Dragila, M.I., Weisbrod, N., 2014. Impact of thermal convection on CO_2 flux
576 across the earth-atmosphere boundary in high-permeability soils. Agric. For.
577 Meteorol. 184, 12–24.
578 Hanson, P.J., Edwards, N.T., Garten, C.T., Andrews, J.A., 2000. Separating root and
579 soil microbial contributions to soil respiration: A review of methods and
580 observations. Biogeochemistry 48, 115–146.
581 He, X., Inoue, T., 2015. Peatland Tank Model for evaluation of shallow groundwater
582 table data without height reference from benchmark. Int. J. Environ. Rural Dev. 6,
583 16–21.
584 Hergoualc'h, K., Verchot, L. V., 2011. Stocks and fluxes of carbon associated with land
585 use change in Southeast Asian tropical peatlands: A review. Global Biogeochem.
586 Cycles 25, doi: 10.1029/2009GB003718.
587 Hirano, T., Jauhiainen, J., Inoue, T., Takahashi, H., 2009. Controls on the carbon
588 balance of tropical peatlands. Ecosystems 12, 873–887.
589 Hirano, T., Kusin, K., Limin, S., Osaki, M., 2014. Carbon dioxide emissions through
590 oxidative peat decomposition on a burnt tropical peatland. Glob. Chang. Biol. 20,
591 555–565.
592 Hooijer, A., Page, S., Jauhiainen, J., Lee, W.A., Lu, X.X., Idris, A., Anshari, G., 2012.
593 Subsidence and carbon loss in drained tropical peatlands. Biogeosciences 9, 1053–
594 1071.
595 Husnain, H., Wigena, I.G.P., Dariah, A., Marwanto, S., Setyanto, P., Agus, F., 2014.

596 CO_2 emissions from tropical drained peat in Sumatra, Indonesia. Mitig. Adapt.
597 Strateg. Glob. Chang. 19, 845–862.
598 IPCC, 2014. 2013 Supplement to the 2006 IPCC Guidelines for National Greenhouse
599 Gas Inventories: Wetlands. Switzerland. URL http://www.ipcc-nggip.iges.or.jp
600 Ishikura, K., Yamada, H., Toma, Y., Takakai, F., Morishita, T., Darung, U., Limin, A.,
601 Limin, S.H., Hatano, R., 2017. Effect of groundwater level fluctuation on soil
602 respiration rate of tropical peatland in Central Kalimantan, Indonesia. Soil Sci.
603 Plant Nutr. 63, 1–13.
604 Itoh, M., Okimoto, Y., Hirano, T., Kusin, K., 2017. Factors affecting oxidative peat
605 decomposition due to land use in tropical peat swamp forests in Indonesia. Sci.
606 Total Environ. 609, 906–915.
607 IUSS Working Group WRB, 2015. World Reference Base for Soil Resources 2014,
608 update 2015 International soil classification system for naming soils and creating
609 legends for soil maps. World Soil Resources Reports No. 106. FAO, Rome.
610 Jauhiainen, J., Hooijer, A., Page, S.E., 2012. Carbon dioxide emissions from an *Acacia*
611 plantation on peatland in Sumatra, Indonesia. Biogeosciences 9, 617–630.
612 Jauhiainen, J., Limin, S., Silvennoinen, H., Vasander, H., 2008. Carbon dioxide and
613 methane fluxes in drained tropical peat before and after hydrological restoration.
614 Ecology 89, 3503–3514.
615 Lai, D.Y.F., Roulet, N.T., Humphreys, E.R., Moore, T.R., Dalva, M., 2012. The effect
616 of atmospheric turbulence and chamber deployment period on autochamber CO_2
617 and CH_4 flux measurements in an ombrotrophic peatland. Biogeosciences 9, 3305–
618 3322.
619 Linn, D.M., Doran, J.W., 1984. Effect of water-filled pore space on carbon dioxide and

620 nitrous oxide production in tilled and nontilled soils. Soil Sci. Soc. Am. J. 48,
621 1267.
622 Maltby, E., Immirzi, P., 1993. Carbon dynamics in peatlands and other wetland soils
623 regional and global perspectives. Chemosphere 27, 999–1023.
624 Marwanto, S., Agus, F., 2014. Is CO_2 flux from oil palm plantations on peatland
625 controlled by soil moisture and/or soil and air temperatures? Mitig. Adapt. Strateg.
626 Glob. Chang. 19, 809–819.
627 Melling, L., Goh, K.J., Chaddy, A., Hatano, R., 2013a. Soil CO_2 fluxes from different
628 ages of oil palm in tropical peatland of Sarawak, Malaysia as influenced by
629 environmental and soil properties. Acta Hortic. 982, 25–35.
630 Melling, L., Hatano, R., Goh, K.J., 2005. Soil CO_2 flux from three ecosystems in
631 tropical peatland of Sarawak, Malaysia. Tellus 57B, 1–11.
632 Melling, L., Yun Tan, C.S., Goh, K.J., Hatano, R., 2013b. Soil microbial and root
633 respirations from three ecosystems in tropical peatland of Sarawak, Malaysia. J.
634 Oil Palm Res. 25, 44–57.
635 Michel, J.C., Rivière, L.M., Bellon-Fontaine, M.N., 2001. Measurement of the
636 wettability of organic materials in relation to water content by the capillary rise
637 method. Eur. J. Soil Sci. 52, 459–467.
638 Miettinen, J., Hooijer, A., Vernimmen, R., Liew, S.C., Page, S.E., 2017. From carbon
639 sink to carbon source: extensive peat oxidation in insular Southeast Asia since
640 1990. Environ. Res. Lett. 12, 24014.
641 Miettinen, J., Shi, C., Liew, S.C., 2016. Land cover distribution in the peatlands of
642 Peninsular Malaysia, Sumatra and Borneo in 2015 with changes since 1990. Glob.
643 Ecol. Conserv. 6, 67–78.

644 Moore, S., Gauci, V., Evans, C.D., Page, S.E., Hall, W., Keynes, M., Wales, E.C.,
645 Road, D., 2011. Fluvial organic carbon losses from a Bornean blackwater river.
646 Biogeosciences 8, 901–909.
647 Murayama, S., Bakar, Z.A., 1996. Decomposition of tropical peat soils. 2. Estimation of
648 in situ decomposition by measurement of CO_2 flux. Japan Agric. Res. Q. 30, 153–
649 158.
650 Page, S.E., Rieley, J.O., Banks, C.J., 2011. Global and regional importance of the
651 tropical peatland carbon pool. Glob. Chang. Biol. 17, 798–818.
652 Price, J., 1997. Soil moisture, water tension, and water table relationships in a managed
653 cutover bog. J. Hydrol. 202, 21–32.
654 R Core Team, 2017. R: A Language and Environment for Statistical Computing. R
655 Foundation for Statistical Computing, Vienna, Austria. URL https://www.r-
656 project.org/
657 Sakata, R., Shimada, S., Arai, H., Yoshioka, N., Yoshioka, R., Aoki, H., Kimoto, N.,
658 Sakamoto, A., Melling, L., Inubushi, K., 2015. Effect of soil types and nitrogen
659 fertilizer on nitrous oxide and carbon dioxide emissions in oil palm plantations.
660 Soil Sci. Plant Nutr. 61, 48–60.
661 Sjögersten, S., Black, C.R., Evers, S., Hoyos-Santillan, J., Wright, E.L., Turner, B.L.,
662 2014. Tropical wetlands: A missing link in the global carbon cycle? Global
663 Biogeochem. Cycles 28, 1371–1386.
664 Stephens, J.C., Stewart, E.H., 1976. Effect of climate on organic soil subsidence, in:
665 Proceedings of the 2nd Symposium on Land Subsidence, Anaheim, California. pp.
666 647–655.
667 Sundari, S., Hirano, T., Yamada, H., Kusin, K., Limin, S., 2012. Effect of groundwater

level on soil respiration in tropical peat swamp forests. J. Agric. Meteorol. 68, 121–134.

van Asselen, S., 2011. The contribution of peat compaction to total basin subsidence : implications for the provision of accommodation space in organic-rich deltas. Basin Res. 23, 239–255.

van Genuchten, M.T., 1980. A closed-form equation for predicting the hydraulic conductivity of unsaturated soils. Soil Sci. Soc. Am. J. 44, 892–898.

Wakhid, N., Hirano, T., Okimoto, Y., Nurzakiah, S., Nursyamsi, D., 2017. Soil carbon dioxide emissions from a rubber plantation on tropical peat. Sci. Total Environ. 581–582, 857–865.

Watanabe, A., Purwanto, B.H., Ando, H., Kakuda, K., Jong, F.-S., 2009. Methane and CO_2 fluxes from an Indonesian peatland used for sago palm (*Metroxylon sagu* Rottb.) cultivation: Effects of fertilizer and groundwater level management. Agric. Ecosyst. Environ. 134, 14–18.

Wösten, J.H.M., Ismail, A.B., van Wijk, A.L.M., 1997. Peat subsidence and its practical implications: a case study in Malaysia. Geoderma 78, 25–36.

686 **Figure legends**

687 Figure 1. Map of the study site

688

689 Figure 2. Allocation of chambers, subsidence pole, and groundwater level (GWL) pipe.
690 CT, FT, and RC represent chamber treatments for close-to-tree (< 2.5 m), far-from-tree
691 (> 3 m), and root-cut plots, respectively.

692

693 Figure 3. Variations in (a) monthly precipitation and (b) monthly mean GWL. Error bars
694 denote 95% confidence intervals.

695

696 Figure 4. Diurnal changes in (a) air and soil temperatures and friction velocity (u^*) and
697 (b) soil CO_2 flux in the CT, FT, and RC plots. Error bars denote 95% confidence intervals.

698

699 Figure 5. Relationship of soil CO_2 efflux with the difference between air and soil
700 temperatures ($\Delta T_{\text{air-soil}}$, air minus soil) or friction velocity (u^*) in the CT, FT, and RC plots.
701 Efflux data were binned into deciles by $\Delta T_{\text{air-soil}}$ or u^*. A linear regression was applied to
702 data at $\Delta T_{\text{air-soil}} < 0$ºC and $u^* < 0.4$ m s^{-1}. Error bars denote 95% confidence intervals.

703

704 Figure 6. Seasonal changes in daily mean soil CO_2 efflux in the CT, FT, and RC plots.
705 Circles and lines represent measured and gap-filled values, respectively. Error bars and
706 the gray area denote 95% confidence intervals of measured and estimated soil CO_2 efflux
707 among chambers, respectively.

708

709 Figure 7. Relationships of daily mean soil CO_2 efflux with (a) GWL and (b) water-filled

710 pore space (WFPS) in the CT, FT, and RC plots.

711

712 Figure 8. Cumulative instantaneous total subsidence (S_{instan}, closed circles), cumulative
713 oxidative subsidence (S_{RH}, open circles) and daily mean GWL (gray line). Error bars
714 denote 95% confidence intervals.

715

716 **Tables**

717 **Table 1**

718 Annual sum of precipitation, and annual mean groundwater level (GWL), water-filled

719 pore space (WFPS, 0–30 cm depth) and soil temperature (5 cm depth).

Variables	Treatment	Mean ± 1SD	
		2015	2016
Precipitation (mm yr^{-1})		3000	2910
GWL (m)	FT	−0.62 ± 0.09	−0.57 ± 0.09
WFPS (m^3 m^{-3})	FT	0.70 ± 0.03	0.69 ± 0.03
	RC	0.68 ± 0.03	0.68 ± 0.03
Soil temperature (°C)	FT	26.8 ± 1.5	27.8 ± 2.2

720 FT: far-from-tree (> 3 m); RC: root-cut

721

Table 2

Results of a multiple regression analysis for hourly soil CO_2 efflux (μmol m^{-2} s^{-1}) with soil temperature (°C), groundwater level (GWL, m), difference between air and soil temperatures ($\Delta T_{air\text{-}soil}$), and friction velocity (u^*, m s^{-1}). Std. coeff. represents the standardized regression coefficient.

Treatment	Predictor	Coefficient	Std. coeff.	*P*-value	R^2
CT	Intercept	2.89		< 0.001	0.128
(*n* = 8618)	Soil temperature	−0.03	−0.014	0.18	
	GWL	−10.2	−0.296	< 0.001	
	$\Delta T_{air\text{-}soil}$	−0.20	−0.197	< 0.001	
	u^*	−0.57	−0.032	< 0.05	
FT	Intercept	−2.91		< 0.001	0.107
(*n* = 9506)	Soil temperature	0.07	0.006	0.09	
	GWL	−7.37	−0.303	< 0.001	
	$\Delta T_{air\text{-}soil}$	−0.08	−0.109	< 0.001	
	u^*	−0.65	−0.049	< 0.001	
RC	Intercept	−1.80		< 0.001	0.064
(*n* = 17617)	Soil temperature	0.002	0.001	< 0.001	
	GWL	−6.37	−0.205	< 0.001	
	$\Delta T_{air\text{-}soil}$	−0.11	−0.125	< 0.001	
	u^*	−0.92	−0.057	< 0.001	

CT: close-to-tree (< 2.5 m); FT: far-from-tree (> 3 m); RC: root-cut

729 **Table 3**

730 Annual cumulative soil CO_2 emissions (mean ± 1 standard deviation (n)) and the ratio of heterotrophic to total soil respiration (R_H/R_S).

731 Mean values with the same letter are not significantly different ($P > 0.05$).

Year	Annual cumulative soil CO_2 emission (kg C m^{-2} yr^{-1})			R_H/R_S ratio	
	CT (R_S)	FT (R_S)	RC (R_H)	RC/CT	RC/FT
2015	1.13 ± 0.63 (3)	0.63 ± 0.30 (4)	0.76 ± 0.24 (8)	0.68	1.20
2016	0.94 ± 0.53 (3)	0.55 ± 0.25 (5)	0.61 ± 0.16 (8)	0.65	1.12
Mean	1.03 ± 0.53 b	0.59 ± 0.26 a	0.69 ± 0.21 ab	0.66	1.16

732 CT: close-to-tree (< 2.5 m); FT: far-from-tree (> 3 m); RC: root-cut

733

Table 4

Annual subsidence as a result of oxidative peat decomposition (R_H) and its contribution to total subsidence. Bulk density and total carbon (C) content of surface peat with 60-cm thickness are shown. The total annual subsidence rate was determined instantaneously from January's measurements and smoothed using Eq. (7). Values are shown as means ± 1 standard deviation.

Year	Annual R_H	Bulk density	Total C content	Subsidence through R_H	Total subsidence rate		Contribution of R_H to subsidence	
	(kg C m^{-2} yr^{-1})	(Mg m^{-3})	(%)	(cm yr^{-1})	(cm yr^{-1})		(%)	
					instantaneous	smoothed	instantaneous	smoothed
2015	0.76 ± 0.24	0.12 ± 0.02	52.8 ± 0.8	1.22 ± 0.45	1.23 ± 0.49	1.83	100	67
2016	0.61 ± 0.16			0.99 ± 0.32	2.02 ± 0.44	1.27	49	78
Mean	0.69 ± 0.21			1.11 ± 0.39	1.62 ± 0.46	1.55	74	72

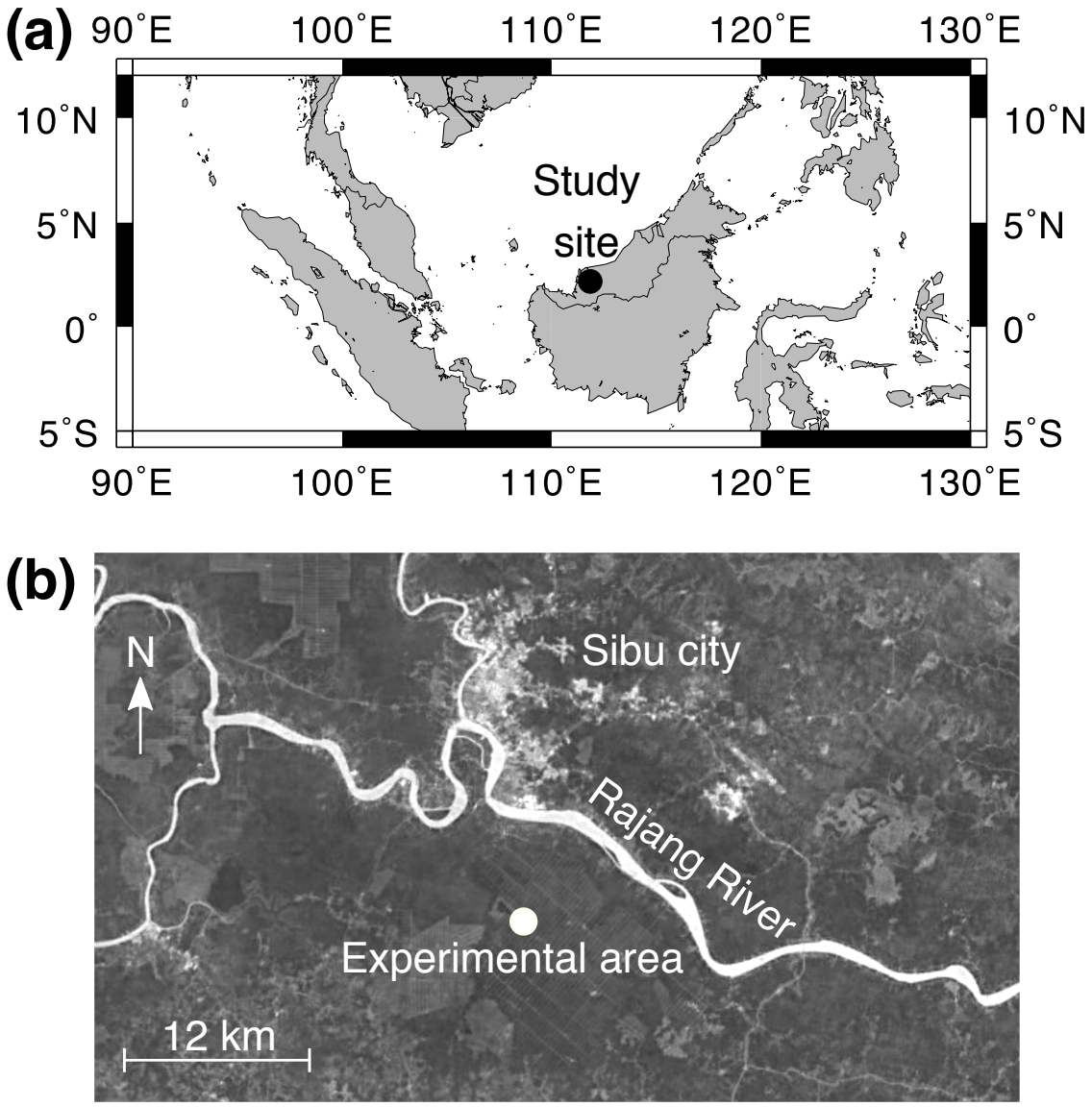
(a)
90˚E
100˚E
110˚E
120˚E
130˚E
10˚N
5˚N
0˚
5˚S
Study
site
(b)
N
Sibu city
Rajang River
Experimental area
12 km

Fig. 1

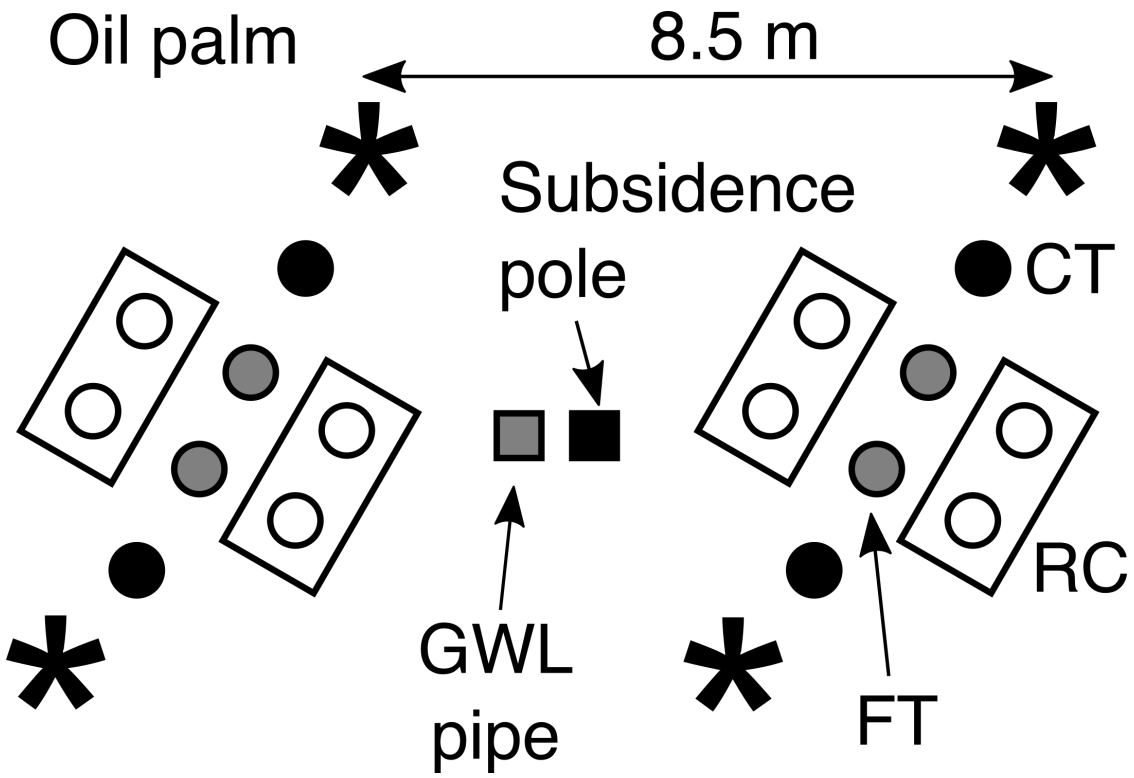

Fig. 2

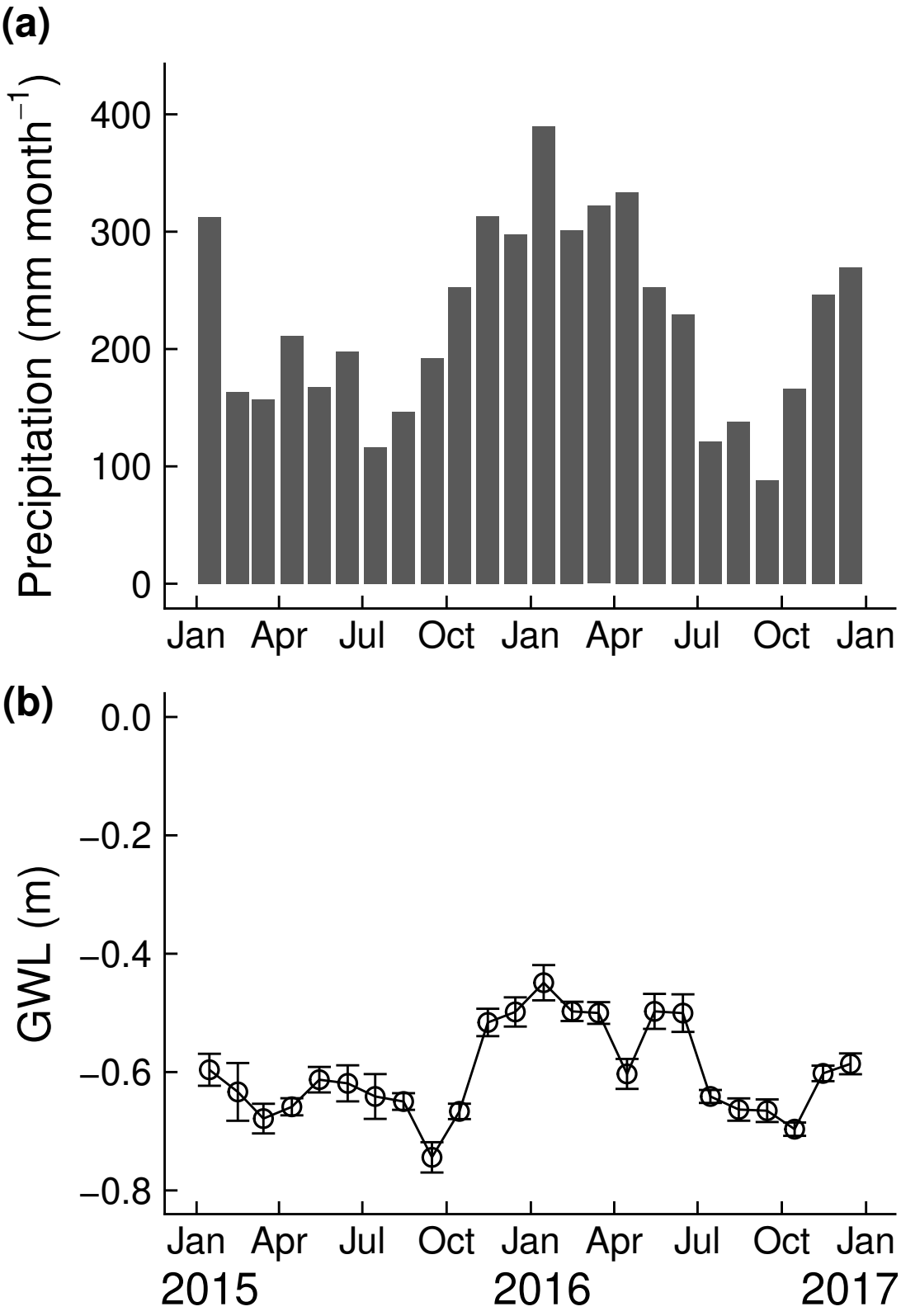
(a)
Precipitation (mm month^{-1})
400
300
200
100
0
Jan
Apr
Jul
Oct
Jan
Apr
Jul
Oct
Jan
(b)
GWL (m)
0.0
−0.2
−0.4
−0.6
−0.8
Jan
Apr
Jul
Oct
Jan
Apr
Jul
Oct
Jan
2015
2016
2017

Fig. 3

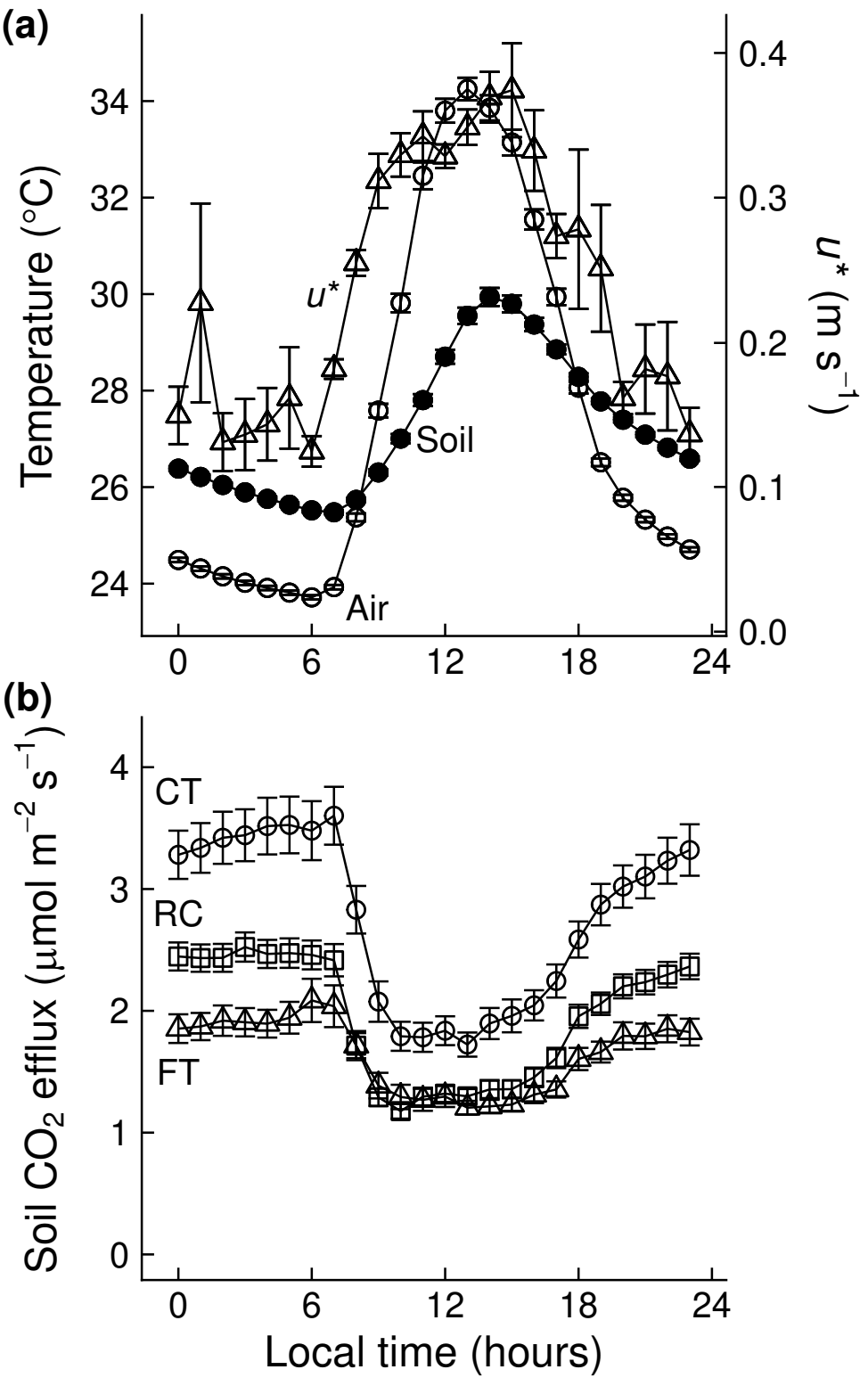
(a)
Temperature (°C)
34
32
30
28
26
24
u*
Soil
Air
0.4
0.3
0.2
0.1
0.0
u* (m s⁻¹)
0
6
12
18
24
(b)
Soil CO2 efflux (μmol m−2 s−1)
CT
RC
FT
4
3
2
1
0
Local time (hours)

Fig. 4

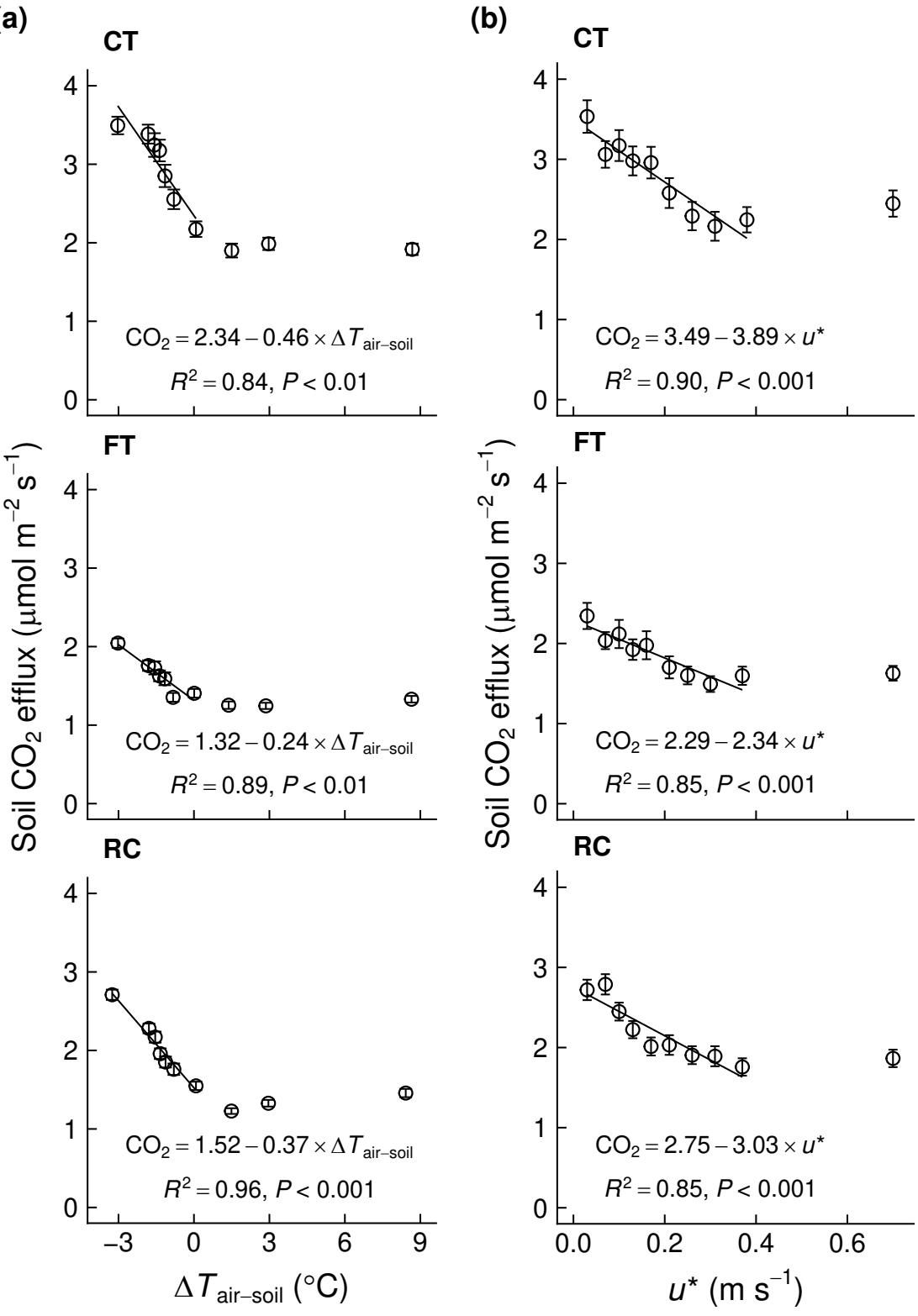
(a)
(b)
CT
FT
RC
Soil CO_2 efflux (μmol m^{-2} s^{-1})
$CO_2 = 2.34 - 0.46 \times \Delta T_{air-soil}$
$R^2 = 0.84$, $P < 0.01$
$CO_2 = 3.49 - 3.89 \times u^*$
$R^2 = 0.90$, $P < 0.001$
$CO_2 = 1.32 - 0.24 \times \Delta T_{air-soil}$
$R^2 = 0.89$, $P < 0.01$
$CO_2 = 2.29 - 2.34 \times u^*$
$R^2 = 0.85$, $P < 0.001$
$CO_2 = 1.52 - 0.37 \times \Delta T_{air-soil}$
$R^2 = 0.96$, $P < 0.001$
$CO_2 = 2.75 - 3.03 \times u^*$
$R^2 = 0.85$, $P < 0.001$
$\Delta T_{air-soil}$ (°C)
u^* (m s^{-1})

Fig. 5

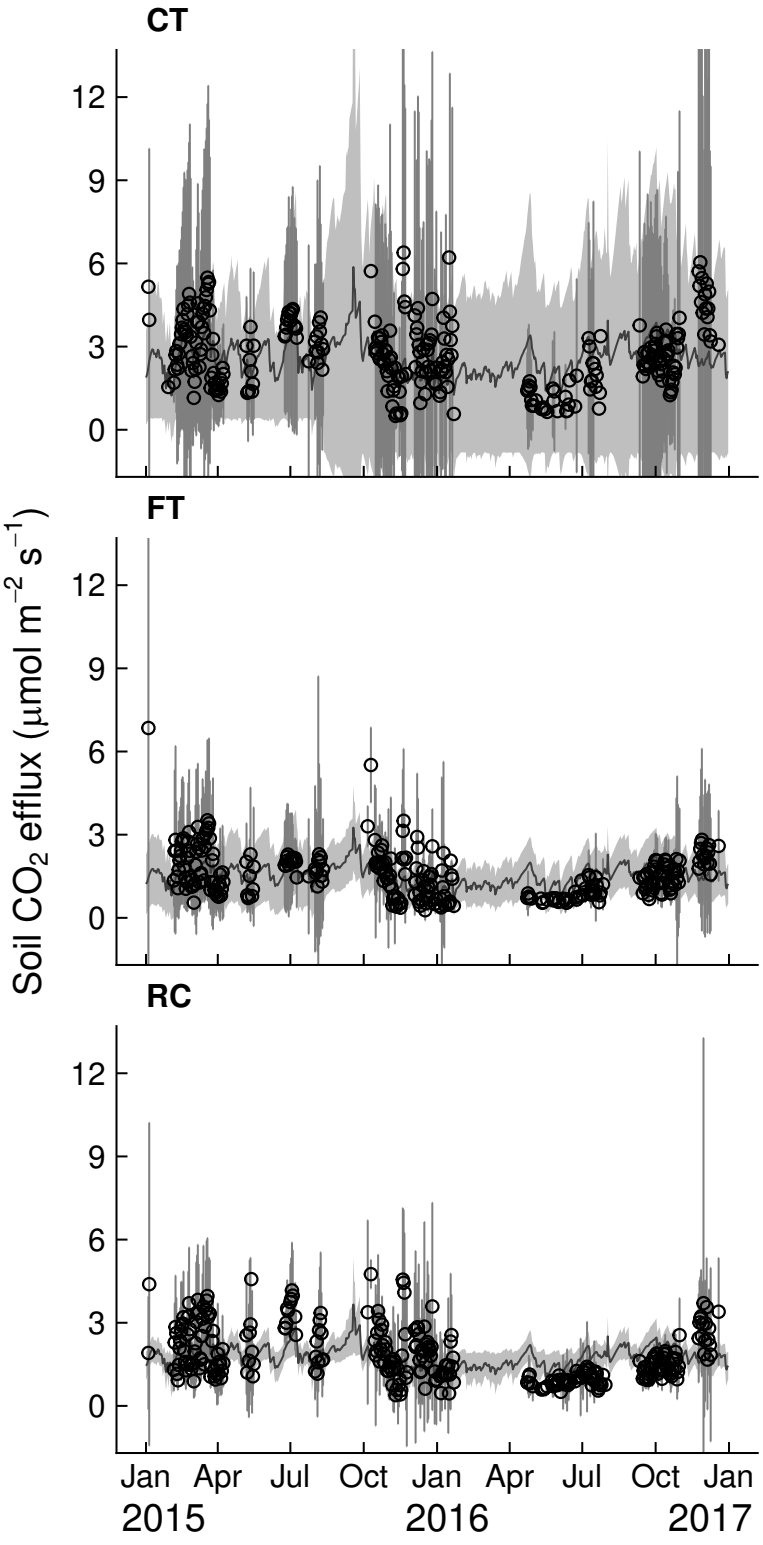
CT
FT
RC
Soil CO_2 efflux (μmol m^{-2} s^{-1})
0
3
6
9
12
Jan
Apr
Jul
Oct
Jan
Apr
Jul
Oct
Jan
2015
2016
2017

Fig. 6

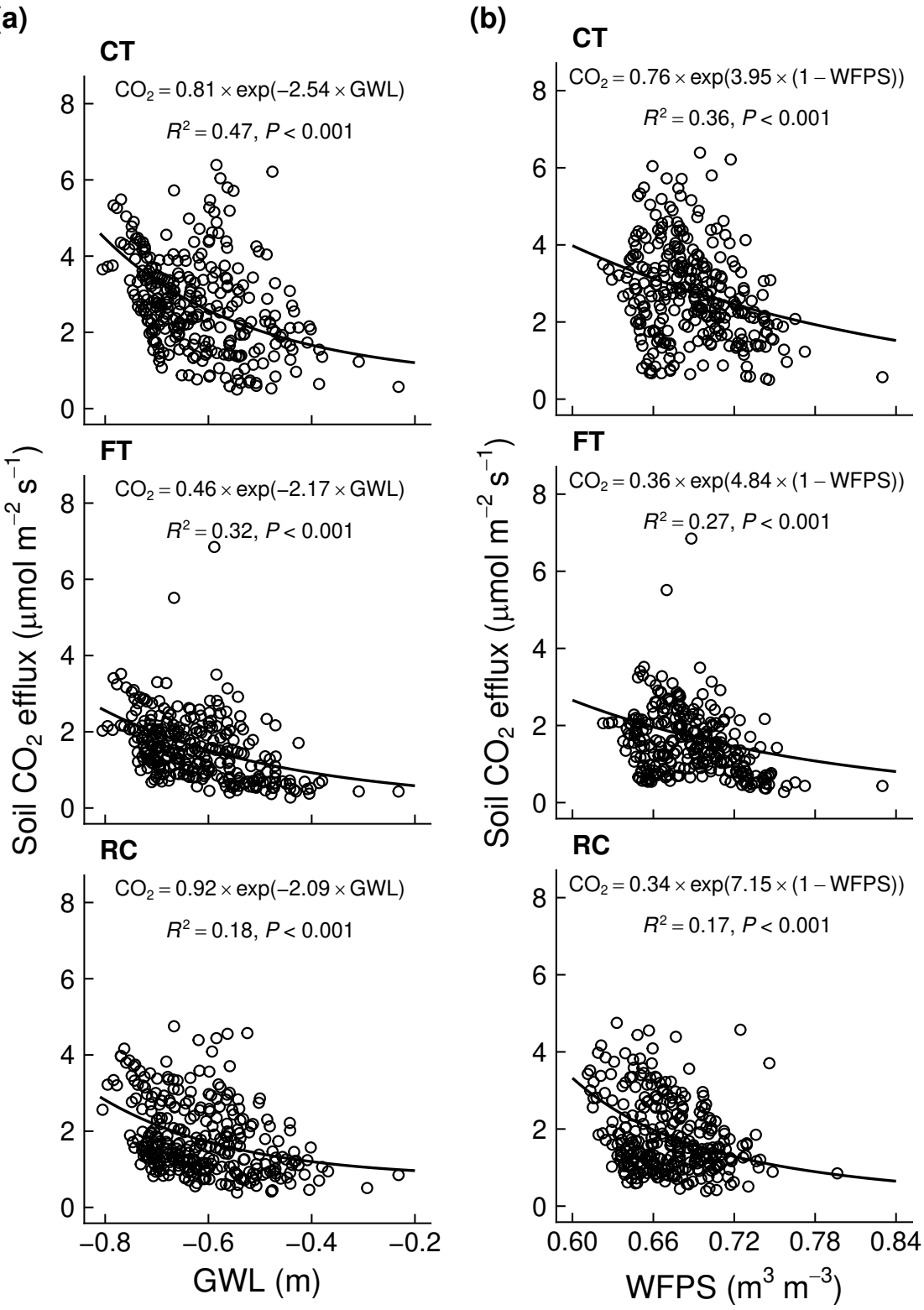
(a)
CT
$CO_2 = 0.81 \times \exp(-2.54 \times GWL)$
$R^2 = 0.47$, $P < 0.001$
FT
$CO_2 = 0.46 \times \exp(-2.17 \times GWL)$
$R^2 = 0.32$, $P < 0.001$
RC
$CO_2 = 0.92 \times \exp(-2.09 \times GWL)$
$R^2 = 0.18$, $P < 0.001$
Soil CO_2 efflux (μmol m^{-2} s^{-1})
GWL (m)
(b)
CT
$CO_2 = 0.76 \times \exp(3.95 \times (1 - WFPS))$
$R^2 = 0.36$, $P < 0.001$
FT
$CO_2 = 0.36 \times \exp(4.84 \times (1 - WFPS))$
$R^2 = 0.27$, $P < 0.001$
RC
$CO_2 = 0.34 \times \exp(7.15 \times (1 - WFPS))$
$R^2 = 0.17$, $P < 0.001$
Soil CO_2 efflux (μmol m^{-2} s^{-1})
WFPS (m^3 m^{-3})

Fig. 7

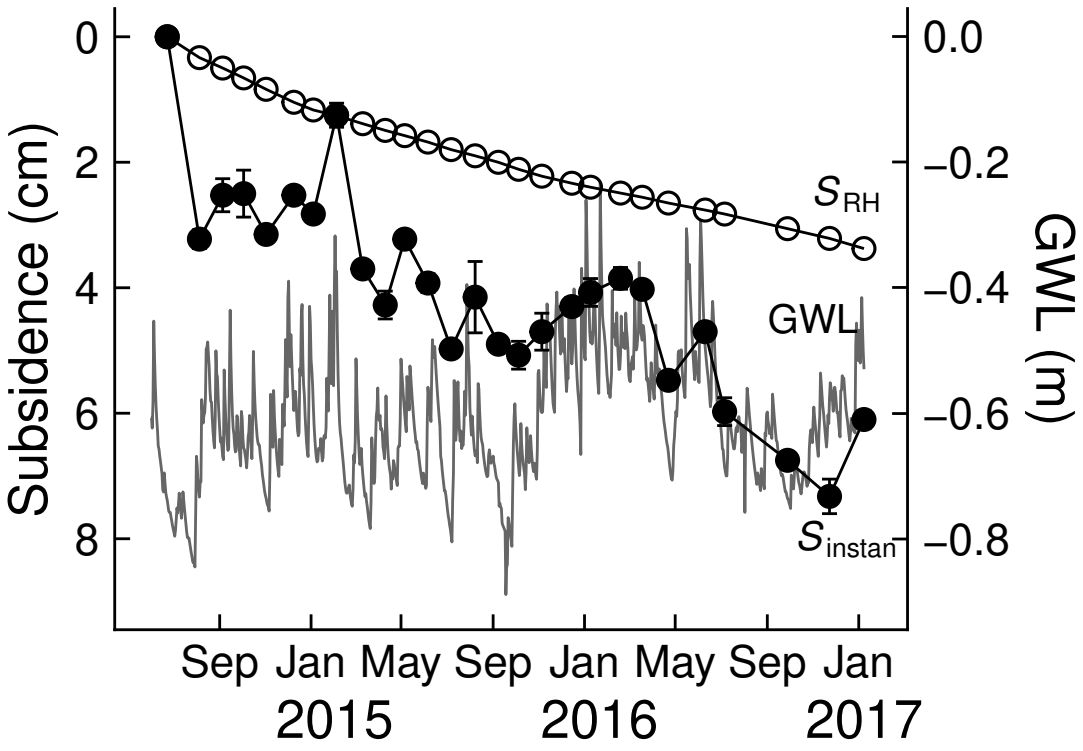
Subsidence (cm)
0
2
4
6
8
0.0
−0.2
−0.4
−0.6
−0.8
GWL (m)
S_{RH}
GWL
S_{instan}
Sep Jan May Sep Jan May Sep Jan
2015
2016
2017

Fig. 8

Supplementary materials

Table S1

Profile of soil physicochemical properties. *n* is sample size at each depth.

Depth (cm)	Bulk density (Mg m^{-3})	Total C (%)	Total N (%)	C:N ratio
n	6	3	3	3
0–10	0.16 ± 0.04	51.5 ± 0.1	2.0 ± 0.00	25.8
10–20	0.11 ± 0.01	52.6 ± 0.1	1.8 ± 0.01	29.2
20–30	0.11 ± 0.01	52.6 ± 0.0	1.9 ± 0.01	27.7
30–40	0.12 ± 0.01	53.0 ± 0.2	1.7 ± 0.01	31.2
40–50	0.10 ± 0.01	53.2 ± 0.3	1.7 ± 0.04	31.3
50–60	0.10 ± 0.01	54.0 ± 0.1	1.6 ± 0.00	33.8
Mean	0.12 ± 0.02	52.8 ± 0.8	1.8 ± 0.13	29.3

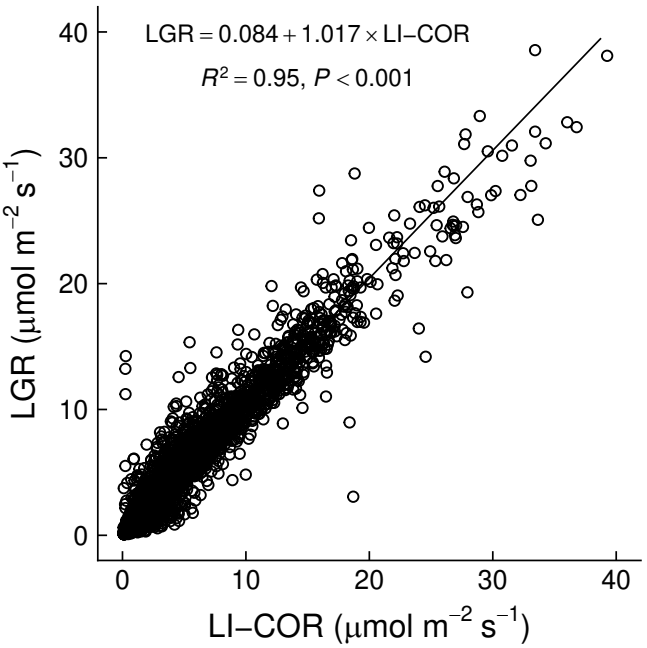

Fig. S1

Comparison of soil CO_2 flux between LI-COR's and LGR's CO_2 analyzer

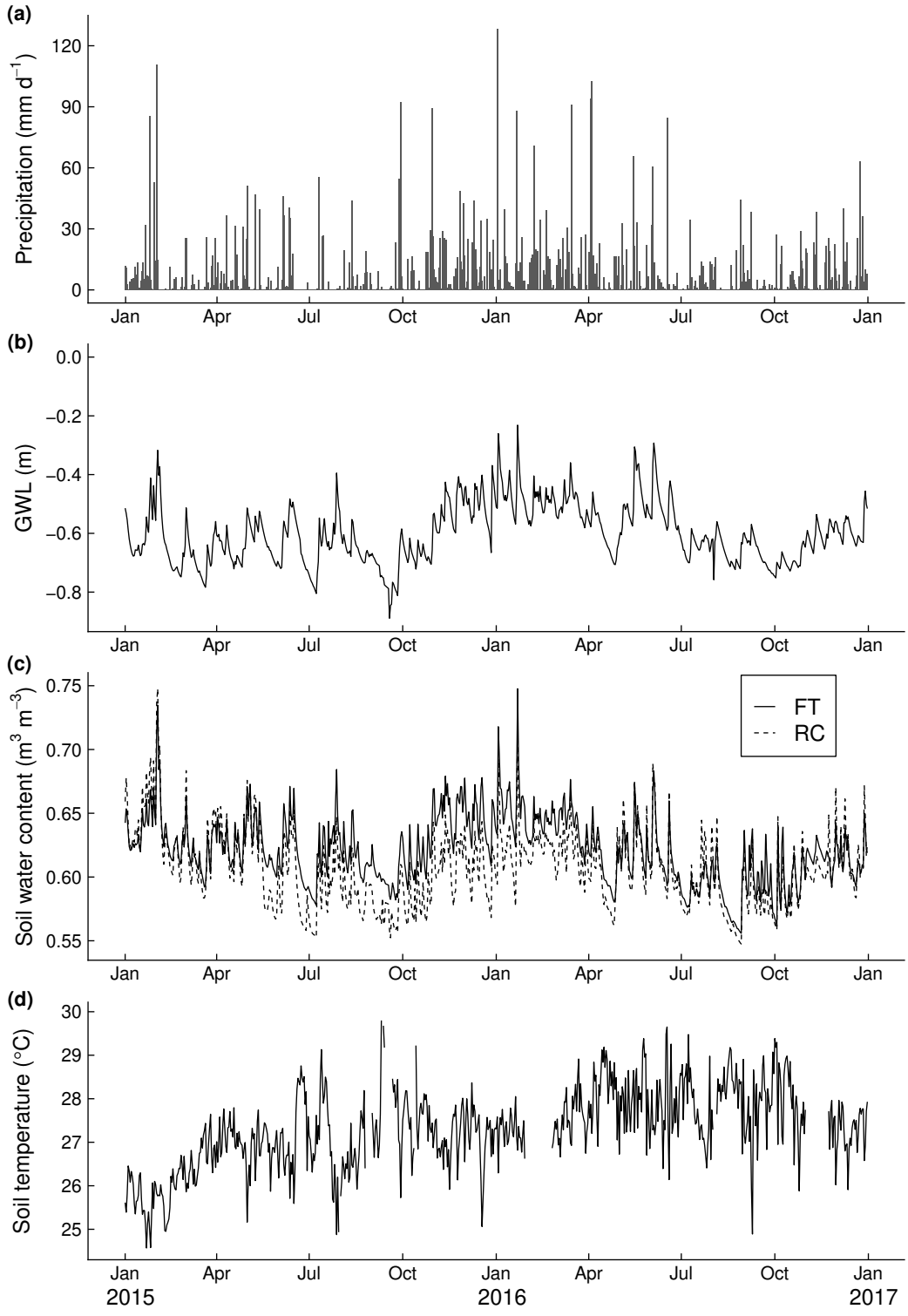

Fig. S2

Seasonal change of (a) daily precipitation, (b) daily mean groundwater level (GWL), (c) daily mean soil water content, and (d) daily mean soil temperature. FT and RC in soil water content represent far-from-tree (> 3 m) and root-cut, respectively.

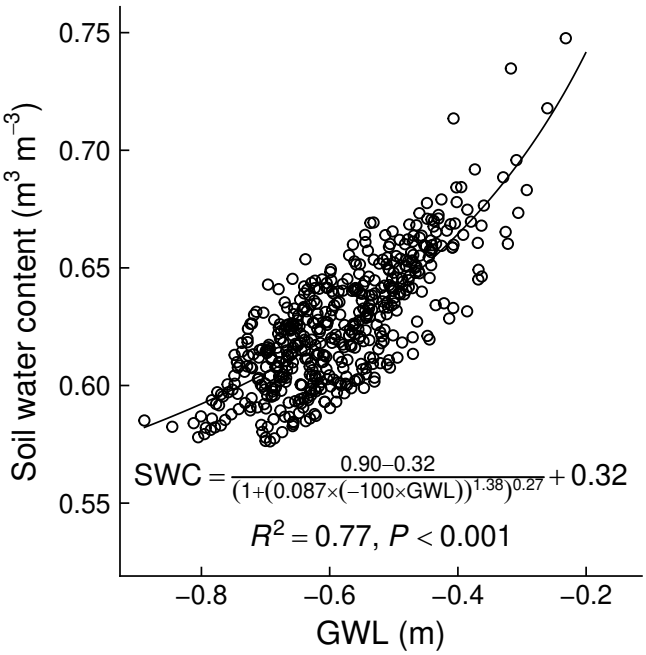

Fig. S3

Relationship between soil water content (SWC) and groundwater level (GWL).